machines

MDPI

Article

Modeling and Analysis of the Turning Performance of an Articulated Tracked Vehicle That Considers the Inter-Unit Coupling Forces

Ningyi Li, Xixia Liu *, Hongqian Chen and Yu Zhang

Department of Vehicle Engineering, Army Academy of Armored Forces, Beijing 100072, China; leeny1992@163.com (N.L.); chenhqaaaf@163.com (H.C.); zhangyuaaaf@163.com (Y.Z.)
* Correspondence: liuaafe@163.com

Abstract: The interactions between ground reaction forces and inter-unit coupling forces add complexity to the study of the turning motion of articulated tracked vehicles (ATVs). To accurately analyze the turning performance of an ATV, this study developed a steady-state steering model that captures the effects of load transfer caused by coupling and centrifugal forces. First, based on vehicle kinematics under skidding conditions, formulas that incorporate parameters for the lateral track displacement were derived to calculate the turning radii of the front and rear units. Then, the track traction forces and turning resistance moments were calculated using the shear stress–shear displacement relationship. Finally, a steady-state steering model on firm ground conditions was developed for the vehicle according to mechanical equilibrium conditions, and the model was validated using previously reported data. Analyses of the results revealed that the coupling forces provided the driving moments for the turning motion by the transfer of the centrifugal and ground reaction forces that acted on the front and rear units. During turning, the rear unit had a larger radius than the front unit, and the minimum swept radius of the ATV was dependent upon the radius of the outer track trajectory of the rear unit. Specifically, at a speed of 3.1 m/s and a steering angle of 35°, the vehicle exhibited a minimum outer swept radius of 8.8 m, requiring a turning space equivalent to a 3.1-m-wide road. The required turning space increased as both the steering angle and speed increased.

Keywords: articulated tracked vehicles; coupling forces; articulation mechanism; turning performance

check for updates

Received: 28 December 2024
Revised: 28 January 2025
Accepted: 30 January 2025
Published: 4 February 2025

Citation: Li, N.; Liu, X.; Chen, H.; Zhang, Y. Modeling and Analysis of the Turning Performance of an Articulated Tracked Vehicle That Considers the Inter-Unit Coupling Forces. *Machines* **2025**, *13*, 118. https://doi.org/10.3390/machines13020118

Copyright: © 2025 by the authors. Licensee MDPI, Basel, Switzerland. This article is an open access article distributed under the terms and conditions of the Creative Commons Attribution (CC BY) license (https://creativecommons.org/licenses/by/4.0/).

1. Introduction

An articulated tracked vehicle (ATV) usually consists of two units joined by an articulation mechanism. During the ATV turning process, the articulation cylinder extends or retracts to create a specific steering angle between the front and rear units, thereby enabling the ATV to perform various turning tasks [1,2]. Due to track slipping and skidding [3,4], it is difficult to accurately predict the turning trajectory of the vehicle using only the steering angle. Additionally, the complex mechanical interactions between the tracks and the ground, as well as between the vehicle components, along with the multiple degrees of freedom that arise from multiple actuators [5], make investigations of the turning dynamics challenging.

Therefore, thorough analyses of the kinematic relationships and mechanical interactions associated with each actuator during the turning process, as well the development of accurate turning dynamic models, are essential for those seeking to understand the turning behavior and analyze the turning performance of ATVs. During the vehicle turning process,

a pair of moments and coupling forces act on the front and rear units at the articulation point. The moments, which are provided by the turning cylinders, are capable of balancing the difference between the turning moments of the front and rear units and altering or maintaining the steering angle. In addition, the coupling forces, which are provided by the cylinders and the articulation frame, primarily transmit the inertial forces from the front and rear units and the interaction forces between the tracks and the ground. The coupling forces of the articulation mechanism cause the weights of the front and rear units to be transferred to the tracks; thus, the normal load and normal pressure distribution of each track change, which in turn affects the tangential force and the tangential moment that the ground exerts on each track. Each unit is in a dynamic equilibrium state, which is influenced by mutual ground reaction forces, inertial forces, moments at the articulation point, and coupling forces [6]. To accurately calculate the kinematic and dynamic parameters of the turning process during ATV turning dynamic modeling, it is essential to consider the load transfer and force transmission caused by the coupling forces of the articulation mechanism.

To date, investigations regarding the turning dynamics of ATVs have been concentrated in countries in the northern hemisphere. Watanabe et al. [7] developed a turning dynamic model for ATVs based on "pull–slip equations" that includes coupling forces and compared the turning maneuverability performance of ATVs with different configurations. Based on the turning model proposed by Watanabe et al., Yamakawa et al. [8,9] calculated and compared the driving forces of each track of ATVs with various differential systems. They also calculated the turning trajectories of the ATVs under load-transfer conditions caused by centrifugal forces and ground slopes. Antonio et al. [10,11] used an arctangent-function model to describe the mechanics of track–ground interactions and developed an ATV turning dynamic model that considered suspension compression. They then used these models to analyze both the steady-state and transient turning behaviors of ATVs. Dong et al. [12,13] developed a turning model based on the relationship between shear stress and shear displacement. This model accounts for the center-of-mass offset between the units, which balances the difference between the turning resistance moments of the front and rear units. While assuming that the normal pressure of each track is uniformly distributed, Yao et al. [14] analyzed the turning moments of an ATV for different steering angles. Wu et al. [15] incorporated soil friction and bulldozing resistance in their modeling approach. Hu et al. [16,17] developed a mathematical model that considers instantaneous soil deformation.

During the process of dynamic modeling, correctly handling the coupling forces between units is of primary importance. Although some studies [7–9] have considered the coupling forces of the articulation mechanism, few covered specific calculation results for these forces. Other studies [10–18] did not consider the load transfer caused by coupling forces. The dynamic models in these previous studies include six unknowns that are related to the motion of the four tracks and the position of the instantaneous center of rotation. However, the solution results contained only the interaction moments between the front and rear units. These models failed to describe the interaction forces between the front and rear units, resulting in insufficient accuracy during vehicle turning motion analyses. To clarify the mechanical relationships between the units, it is necessary to solve the lateral and longitudinal components of the coupling forces, along with eight unknows generated. However, this aspect of the research has rarely been reported.

Secondly, during the process of dynamic modeling, determining which model to use for describing the interaction forces between the track and the ground is critical. Various track–ground contact models have been developed by researchers, ranging from the early Coulomb friction law [19,20] and pull–slip equations [7–9,21,22] to an arctangent-function

model [10,11,23,24], aiming to accurately calculate the ground forces exerted on the tracks. However, the shear stress–shear displacement relationship proposed by Wong et al. [25,26] is considered to be a more reasonable contact model so far [27–29].

Meanwhile, current research on the turning performance of ATVs remains limited. However, extensive studies have been conducted on wheeled articulated vehicles, multi-axle vehicles, and general passenger cars. In the realm of wheeled articulated vehicle handling, Islam et al. [30] investigated the interaction between the trailer and transmission system of articulated heavy vehicles and introduced a driver model to design an effective active trailer-steering system. Vella et al. [31] established a multi-body dynamic simulation model of heavy commercial vehicles using Admas/Car to analyze vehicle cornering maneuvers. Wu and Hai [32] developed a linear yaw model of multi-axle steering tractors and full trailers, developing methods to improve directional response characteristics through active multi-axle steering systems.

Additionally, some studies have explored the impact of curve maneuvering and road surface conditions on vehicle control strategies. Gao and Gordan [33] proposed an optimal control method based on a nonlinear particle model to prevent vehicle departure from roads on curves. Wang et al. [34] combined a dynamic model with camera-based curvature estimation techniques to enhance the driving performance of autonomous vehicles on curves. Bakibillah et al. [35] focused on optimizing driving strategies to reduce energy consumption and carbon emissions while driving on curved roads. Zheng et al. [36] evaluated the braking stability of autonomous vehicles on curved sections, particularly focusing on the influence of asphalt pavement adhesion properties on braking performance.

However, research on stable turning capabilities of vehicles under various motion states, especially concerning minimum sweep radius and turning space for articulated tracked vehicles, remains scarce.

Given the existing research gaps, the objective of this study is to provide a more precise and comprehensive modeling and analytical approach for understanding the turning behavior and performance of ATVs. The main contribution of this research lies in the development of a steady-state turning dynamic model and turning performance analysis method considering the inter-unit coupling forces. This model accounts for the effects of the coupling and centrifugal forces on the normal load and ground contact pressure distribution of each track. It also includes the lateral, longitudinal, and yaw motions of the front unit, the rotation of the rear unit relative to that of the front unit, the rotations of the four drive wheels, and the coupling forces at the articulation point. Using a specific ATV as a case study, calculations were performed on firm ground conditions and the theoretical model was validated using data from the existing literature. The effects of the coupling forces on the turning radii, articulation moments, and track normal loads were examined under various turning conditions with different steering angles and speeds. Additionally, the turning performance of the vehicle was assessed using calculations of the turning radius ratio, the minimum swept radius, and the turning space.

The rest of this paper is organized as follows. Section 2 describes the kinematic model of the ATV turning process, covering unit motion, track sliding speed, and track shear displacement. Section 3 details the dynamic model, which considers inter-unit coupling forces. In Section 4, we validate the model using previously reported data and discuss the rotation center changes and the calculation results of coupling forces. Section 5 explores the impact of coupling forces on turning radii, normal loads, and articulation moments. Finally, Section 6 analyzes turning performance metrics such as radius ratio and minimum swept radius, while Section 7 summarizes our findings.

2. Kinematic Model of the ATV Turning Process

2.1. Assumptions

During the modeling of the ATV turning motion, three assumptions were made as follows:

1. The turning motion was performed on a flat surface, and unit tilting caused by terrain factors was not considered.
2. The centers of mass of the front and rear units coincided with the geometric centers of the respective units.
3. The effects of air resistance, track width, and suspension travel were not considered.

2.2. Definition of the Coordinate Systems

The coordinate systems and kinematic relationships used for the ATV turning motion are depicted in Figure 1. In the figure, subscript i (where i = 1, 2) is used to distinguish between the front and rear units, while subscript j (where j = 1, 2) is used to distinguish between the outer and inner tracks. The masses of the front and rear units are denoted by m_i, the lengths of the track–ground contact sections are denoted by L_i, and the distances between the articulation point, O_A, and the centers of mass, o_i, of the front and rear units are represented by l_i. The track center distances are both denoted by B, while both track widths are represented by b. In Figure 1, OXY represents the global coordinate system, which is fixed to the ground, while $o_1x_1y_1$ and $o_2x_2y_2$ are local coordinate systems that are affixed to the mass centers of the front and rear units at o_i.

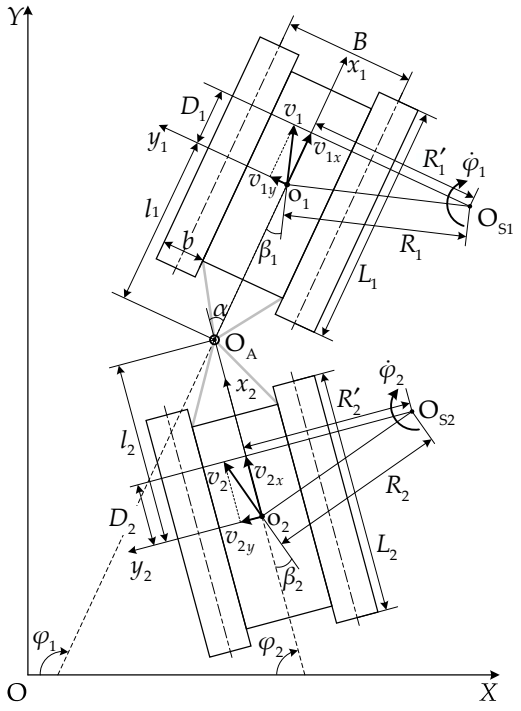


Figure 1. Coordinate systems and kinematic relationships established for the ATV during the turning process.

The speeds of the centers of mass of the front and rear units are represented by v_i, and the longitudinal and lateral speed components are denoted by v_{ix} and v_{iy}, respectively. The yaw angles of the front and rear units are denoted by φ_i, and the side slip angles are represented by β_i. The instantaneous turning centers are denoted by O_{Si}, and, when the vehicle is engaged in steady-state turning, the turning centers of the front and rear units coincide.

The distances between O_{Si} and o_i are the instantaneous turning radii, R_i. The lateral distances between O_{Si} and the longitudinal axes of the units are denoted by R'_i. The longitudinal offsets of the instantaneous turning centers caused by lateral track slippage are denoted as D_i, and the steering angle between the front and rear units at the articulation point is represented by α.

2.3. Unit Motion

As shown in Figure 1, when the ATV turns with a steering angle of α, the instantaneous turning radius can be expressed by Equation (1):

$$R_i = \frac{v_i}{\dot{\varphi}_i} \tag{1}$$

The lateral distance, R'_i, can be expressed by Equation (2):

$$R'_i = R_i \cos \beta_i \tag{2}$$

The longitudinal and lateral speed components of v_x are provided in Equation (3):

$$\begin{cases} v_{ix} = R'_i \dot{\varphi}_i \\ v_{iy} = D_i \dot{\varphi}_i \end{cases} \tag{3}$$

Based on the speed relationships at the articulation point, v_{2x} and v_{2y} can be expressed in terms of v_{1x} and v_{1y}, as shown in Equation (4):

$$\begin{cases} v_{2x} = v_{1x} \cos \alpha + \left(v_{1y} + \dot{\varphi}_1 l_1\right) \sin \alpha \\ v_{2y} = \left(v_{1y} + \dot{\varphi}_1 l_1\right) \cos \alpha - v_{1x} \sin \alpha + \left(\dot{\varphi}_1 - \dot{\alpha}\right) l_2 \end{cases} \tag{4}$$

The side slip angles of the front and rear units can be expressed by Equation (5):

$$\beta_i = \arctan \frac{v_{iy}}{v_{ix}} \tag{5}$$

The relationships between the yaw angles and α are provided in Equation (6):

$$\begin{cases} \alpha = \varphi_1 - \varphi_2 \\ \dot{\alpha} = \dot{\varphi}_1 - \dot{\varphi}_2 \end{cases} \tag{6}$$

When the ATV is engaged in steady-state turning, α remains constant; thus, Equation (7) is applicable as follows:

$$\begin{cases} \dot{\alpha} = 0 \\ \dot{\varphi}_1 = \dot{\varphi}_2 \end{cases} \tag{7}$$

Substituting Equation (3) into (4) yields Equation (8):

$$\begin{cases} v_{2x} = \dot{\varphi}_1 \left(R'_1 \cos \alpha + D_1 \sin \alpha + l_1 \sin \alpha\right) \\ v_{2y} = \dot{\varphi}_1 \left(D_1 \cos \alpha - R'_1 \sin \alpha + l_1 \cos \alpha + l_2\right) \end{cases} \tag{8}$$

In addition, combining Equations (3), (4), and (8) yields Equation (9):

$$\begin{cases} v_{1x} = \left[\left(1 + \frac{l_1}{D_1}\right) \cot \alpha + \frac{l_2 - D_2}{D_1 \sin \alpha}\right] v_{1y} \\ v_{2x} = \left[\left(1 + \frac{l_1}{D_1}\right) \sin \alpha + \frac{(D_1 + l_1) \cos \alpha - (D_2 - l_2)}{D_1 \tan \alpha}\right] v_{1y} \end{cases} \tag{9}$$

Expressions for R_i as functions of the lateral slip parameters of the tracks are obtained by combining Equations (1) and (9):

$$\begin{cases} R_1 = \sqrt{\left(\frac{l_1+D_1}{\tan\alpha} + \frac{l_2-D_2}{\sin\alpha}\right)^2 + {D_1}^2} \\ R_2 = \sqrt{\left(\frac{l_1+D_1}{\sin\alpha} + \frac{l_2-D_2}{\tan\alpha}\right)^2 + {D_2}^2} \end{cases} \tag{10}$$

According to Equation (9), the R_i values are primarily influenced by the longitudinal offsets, D_i, the vehicle structural parameters, l_i, and the kinematic parameter α. When $D_i = 0$, Equation (10) becomes the expression for the theoretical turning radius under no-skid conditions. This result is consistent with the results derived from the geometric relationship by Lin [18].

2.4. Track Sliding Speed and Shear Displacement

2.4.1. Sliding Speed

During the turning motion of the ATV, the track motion is composed of the planar motion of the unit relative to the ground and the wrapping motion of the tracks relative to the unit. A sliding speed analysis of a track element at the track–ground interface during the ATV turning motion is depicted in Figure 2.

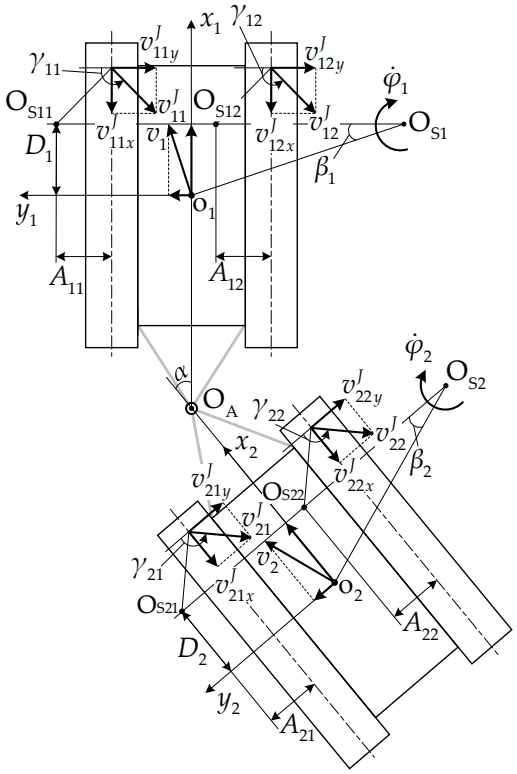


Figure 2. Sliding speed of a track element at the track–ground interface during the ATV turning process.

For point $k_{ij}(x_i, 0)$, which lies on the track longitudinal axis at the track–ground interface, the implicated speed components are $v_{\mathrm{k}ijx}$ and $v_{\mathrm{k}ijy}$, which can be expressed by Equation (11):

$$\begin{cases} v_{\mathrm{k}ijx} = v_{ix} \pm \frac{B}{2}\dot{\varphi}_i \\ v_{\mathrm{k}ijy} = -(x_i - D_i)\dot{\varphi}_i \end{cases} \tag{11}$$

The radius of the pitch circle of each track drive wheel is denoted by r, the angular speeds of the drive wheels are represented by ω_{ij}, and the wrapping speeds, $v_{\mathrm{d}ij}$, of track ij relative to the units can be expressed by Equation (12):

$$v_{\mathrm{d}ij} = r\omega_{ij} \tag{12}$$

The longitudinal and lateral components of the sliding speed at k_{ij} are denoted by $v^J_{\mathrm{k}ijx}$ and $v^J_{\mathrm{k}ijy}$, respectively, and can be expressed by Equation (13):

$$\begin{cases} v^J_{\mathrm{k}ijx} = \dot{\varphi}_i\left(R'_i \pm \frac{B}{2}\right) - r\omega_{ij} \\ v^J_{\mathrm{k}ijy} = -(x_i - D_i)\dot{\varphi}_i \end{cases} \tag{13}$$

Figure 2 demonstrates that the longitudinal sliding of track ij causes a lateral displacement, A_{ij}, of the instantaneous center of speed. This displacement can be expressed by Equation (14):

$$A_{ij} = -\frac{v^J_{\mathrm{k}ijx}}{\dot{\varphi}_i} = -\left(R'_i \pm \frac{B}{2} - \frac{r\omega_{ij}}{\dot{\varphi}_i}\right) \tag{14}$$

The slip angles, γ_{ij}, at k_{ij} can be expressed by Equation (15):

$$\begin{cases} \sin\gamma_{ij} = \frac{v^J_{\mathrm{k}ijx}}{v^J_{kij}} = \frac{-A_{ij}}{\sqrt{{A_{ij}}^2 + (x_i - D_i)^2}} \\ \cos\gamma_{ij} = \frac{v^J_{\mathrm{k}ijy}}{v^J_{kij}} = \frac{-x_{ij}}{\sqrt{{A_{ij}}^2 + (x_i - D_i)^2}} \end{cases} \tag{15}$$

The direction cosine matrix, $\boldsymbol{P}$, for the local unit coordinate systems with respect to the global coordinate system is provided in Equation (16):

$$\boldsymbol{P} = \begin{bmatrix} -\cos\varphi_i & -\sin\varphi_i \\ \sin\varphi_i & -\cos\varphi_i \end{bmatrix} \tag{16}$$

Subsequently, the sliding speed components, $V^J_{\mathrm{k}ijX}$ and $V^J_{\mathrm{k}ijY}$, of k_{ij} in the global coordinate system can be expressed by Equation (17):

$$\begin{cases} V^J_{\mathrm{k}ijX} = -\left[\left(R'_i \pm \frac{B}{2}\right)\dot{\varphi}_i - r\omega_{ij}\right]\cos\varphi_i + (x_i - D_i)\dot{\varphi}_i\sin\varphi_i \\ V^J_{\mathrm{k}ijY} = \left[\left(R'_i \pm \frac{B}{2}\right)\dot{\varphi}_i - r\omega_{ij}\right]\sin\varphi_i + (x_i - D_i)\dot{\varphi}_i\cos\varphi_i \end{cases} \tag{17}$$

2.4.2. Shear Displacement

The time, t, required for point k_{ij} to move from $(L_i/2, 0)$ in front of the track to $(x_i, 0)$ is provided in Equation (18):

$$t = \int_{x_i}^{\frac{L_i}{2}} \frac{\mathrm{d}x_i}{v_{\mathrm{d}ij}} = \frac{L_i/2 - x_i}{r\omega_{ij}} \tag{18}$$

The shear displacements, $J_{X_{ij}}$ and $J_{Y_{ij}}$, which are generated by track ij in the X- and Y-directions of the global coordinate system, respectively, can be expressed by Equation (19):

$$\begin{cases} J_{X_{ij}} = \int_0^t V_{kijX}^J \mathrm{d}t = \int_{x_i}^{\frac{L_i}{2}} V_{kijX}^J \dfrac{\mathrm{d}x_{ij}}{r\omega_{ij}} \\ J_{Y_{ij}} = \int_0^t V_{kijY}^J \mathrm{d}t = \int_{x_i}^{\frac{L_i}{2}} V_{kijY}^J \dfrac{\mathrm{d}x_{ij}}{r\omega_{ij}} \end{cases} \tag{19}$$

Integrating Equation (19) yields Equation (20):

$$\begin{cases} J_{X_{ij}} = -\left(R_i' \pm \dfrac{B}{2}\right) \sin\left(\dfrac{L_i - 2x_i}{2R_i' \pm B + 2A_{ij}}\right) \\ \quad -(x_i - D_i)\cos\left(\dfrac{L_i - 2x_i}{2R_i' \pm B + 2A_{ij}}\right) + \left(\dfrac{L_i}{2} - D_i\right) \\ J_{Y_{ij}} = -\left(R_i' \pm \dfrac{B}{2}\right)\left[\cos\left(\dfrac{L_i - 2x_i}{2R_i' \pm B + 2A_{ij}}\right) - 1\right] \\ \quad +(x_i - D_i)\sin\left(\dfrac{L_i - 2x_i}{2R_i' \pm B + 2A_{ij}}\right) \end{cases} \tag{20}$$

The total shear displacements, J_{ij}, resulting from the sliding of track ij can be expressed by Equation (21):

$$J_{ij} = \sqrt{{J_{ijX}}^2 + {J_{ijY}}^2} \tag{21}$$

3. Dynamic ATV Turning Model

3.1. Track–Ground Modeling That Considers Inter-Unit Coupling Forces

The normal loads and normal pressure distributions for the ATV tracks are depicted in Figure 3. The normal loads of the tracks are denoted by F_{ijz}, while the longitudinal and lateral components of the inertial forces acting on the front and rear units are denoted by F_{ix}^{C} and F_{iy}^{C}, respectively. The longitudinal and lateral components of the coupling forces are represented by $F_{\mathrm{A}ix}$ and $F_{\mathrm{A}iy}$, respectively.

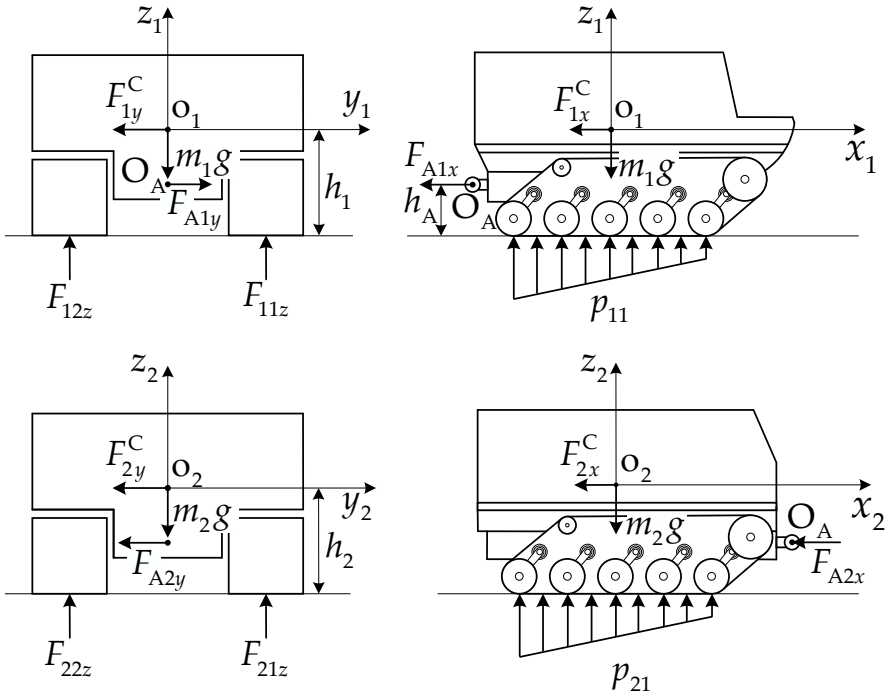


Figure 3. Normal loads and pressure distributions of the tracks at the track–ground interface.

3.1.1. Normal Loads of the Tracks

According to the moment equilibrium relationships at the track centerlines shown in Figure 3, F_{ijz} can be expressed by Equation (22):

$$\begin{cases} F_{1jz} = \frac{1}{2}m_1 g \mp \frac{1}{B}\left(F_{1y}^{C}h_1 - F_{A1y}h_A\right) \\ F_{2jz} = \frac{1}{2}m_2 g \mp \frac{1}{B}\left(F_{2y}^{C}h_2 + F_{A2y}h_A\right) \end{cases} \tag{22}$$

where h_A represents distance from O_A to the ground and h_i is distance from o_i to the ground.

3.1.2. Normal Pressure Distributions

The normal pressure distribution between a track and the ground can be described using a linear distribution model. By neglecting the effects of the track width and changes in the suspension travel, the normal pressure distribution functions, p_{ij}, for the tracks are functions of x_i only, while h_A remains constant. According to the force and moment equilibrium relationships depicted in Figure 3, p_{ij} can be expressed by Equation (23):

$$p_{ij} = \frac{F_{ijz}}{bL_i} - \frac{6}{bL_i{}^3}\left(F_{ix}^{C}h_i + F_{Aix}h_A\right)x_i \tag{23}$$

3.1.3. Shear Forces and Shear Moments

According to the track–ground interaction model proposed by Wong [19], the interaction force between the track and the ground can be modeled by the shear displacement–shear stress relationship. When track sinkage and bulldozing effect are not considered, shear stress is assumed to be an exponential function of shear displacement and can be expressed by Equation (24):

$$\tau = \tau_{max}\left(1 - e^{-J/K}\right) \tag{24}$$

where τ represents the shear stress, τ_{max} is the maximum shear stress, J is the shear displacement, and K represents the shear deformation parameter.

Under firm ground conditions and with adhesion between the track and ground neglected, the relationship between the shear stress and the normal pressure can be expressed by Equation (25):

$$\tau = p\mu\left(1 - e^{-J/K}\right) \tag{25}$$

where p is the normal pressure.

For a differential element of area dA_{ij} at the track–ground interface of track ij, the longitudinal force component, dF_{ijx}^{J}, and lateral force component, dF_{ijy}^{J}, can be expressed by Equation (26):

$$\begin{cases} dF_{ijx}^{J} = -\tau \sin\gamma_{ij} dA_{ij} = -p_{ij}\mu(1 - e^{-J_{ij}/K})\sin\gamma_{ij} dx_{ij} dy_{ij} \\ dF_{ijy}^{J} = -\tau \cos\gamma_{ij} dA_{ij} = -p_{ij}\mu(1 - e^{-J_{ij}/K})\cos\gamma_{ij} dx_{ij} dy_{ij} \end{cases} \tag{26}$$

The total longitudinal shear force, F_{ijx}^{J}, and the total lateral shear force, F_{ijy}^{J}, acting on track ij can be expressed by Equation (27):

$$\begin{cases} F_{ijx}^{J} = \int dF_{ijx}^{J} = -\int_{-L/2}^{L/2} bp_{ij}\mu\left(1 - e^{-J_{ij}/K}\right)\sin\gamma_{ij} dx_i \\ F_{ijy}^{J} = \int dF_{ijy}^{J} = -\int_{-L/2}^{L/2} bp_{ij}\mu\left(1 - e^{-J_{ij}/K}\right)\cos\gamma_{ij} dx_i \end{cases} \tag{27}$$

The longitudinal shear moment, M_{ijx}^{J}, and the lateral shear moment, M_{ijy}^{J}, around the rotation center, O_{vi}, can be expressed by Equation (28):

$$\begin{cases} M_{ijx}^{J} = -\int_{-L/2}^{L/2} \left(\frac{B}{2} \pm y_i\right) b p_{ij} \mu \left(1 - e^{-J_{ij}/K}\right) \sin \gamma_{ij} \mathrm{d}x_i \\ M_{ijy}^{J} = -\int_{-L/2}^{L/2} x_i b p_{ij} \mu \left(1 - e^{-J_{ij}/K}\right) \cos \gamma_{ij} \mathrm{d}x_i \end{cases} \tag{28}$$

3.2. Track Motion Resistance

3.2.1. External Motion Resistance

The external track motion resistance, F_{ij}^{f}, can be expressed by Equation (29):

$$F_{ij}^{f} = F_{ijz} f_r \tag{29}$$

where f_r is the external motion resistance coefficient, which usually has a value in the 0.02–0.03 range [37]. In this study, f_r had a value of 0.025.

3.2.2. Internal Rolling Resistance

The driving dynamics of the track system are illustrated in Figure 4. In this model, track *ij* is subjected to a longitudinal shear force from the ground, a driving force from the driving wheel, a rolling resistance from the load wheel, and an output torque, T_{ij}, from the driving wheel. This output torque can be calculated using Equation (30):

$$T_{ij} = F_{ijx}^{J} r + I_{\mathrm{d}} \dot{\omega}_{ij} + \sum_{k=1}^{N_i} \left[I_{\mathrm{w}} \dot{\omega}_{\mathrm{w}ijk} + q_{ijkz} \left(f_0 + f_s v_{ijk}\right) r \right] \tag{30}$$

where I_{d} represents the moment of inertia of the driving wheel, I_{w} is the moment of inertia of the load wheel, $\dot{\omega}_{\mathrm{w}ijk}$ denotes the rolling angular speed of the k_{th} load wheel, v_{ijk} is the rolling linear speed of the k_{th} load wheel, and f_0 and f_s are empirical coefficients, which had values of 0.03 and 0.00015, respectively.

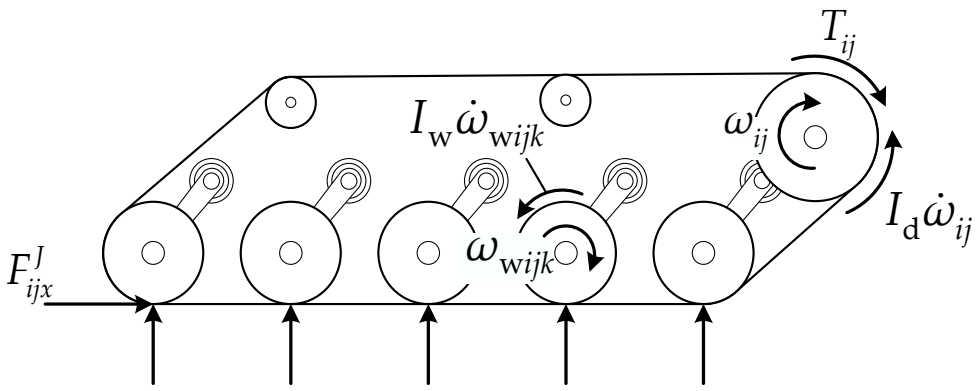


Figure 4. Driving dynamics of the track system.

3.3. Driving Method

An ATV typically utilizes a driving method that combines central and axle differentials, as shown in Figure 5. The engine is in the front unit, and power is distributed through the gearbox and central differential. The power for the front unit passes through the front axle differential and reducer to reach the drive wheels. The power for the rear unit travels through the universal joint shaft at the articulation mechanism, then through the rear axle differential and reducer to reach the drive wheels.

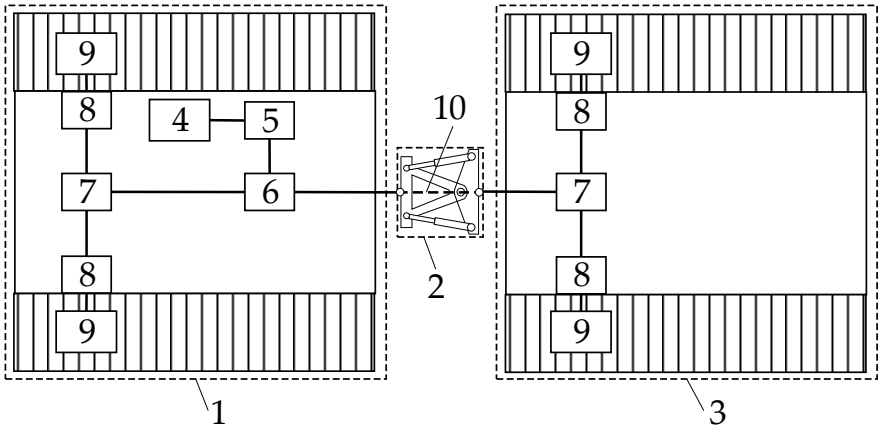


Figure 5. Schematic of the ATV driving method: (**1**) front unit, (**2**) articulation mechanism, (**3**) rear unit, (**4**) engine, (**5**) gearbox, (**6**) central differential, (**7**) axle differential, (**8**) reducer, (**9**) drive wheel, and (**10**) universal drive shaft.

During steady-state turning using the driving method presented above, all four tracks have the same driving force, F_{dij}:

$$F_{d11} = F_{d12} = F_{d21} = F_{d22} \tag{31}$$

3.4. Turning Dynamic Equations

The force diagram for an ATV during a turning motion is presented in Figure 6. The force equilibrium conditions at the articulation point lead to Equation (32):

$$\begin{cases} F_{A1x} = F_{A2y}\sin\alpha - F_{A2x}\cos\alpha \\ F_{A1y} = F_{A2x}\sin\alpha + F_{A2y}\cos\alpha \\ M_1 = M_2 \end{cases} \tag{32}$$

where M_i represents the moment provided by the articulation mechanism.

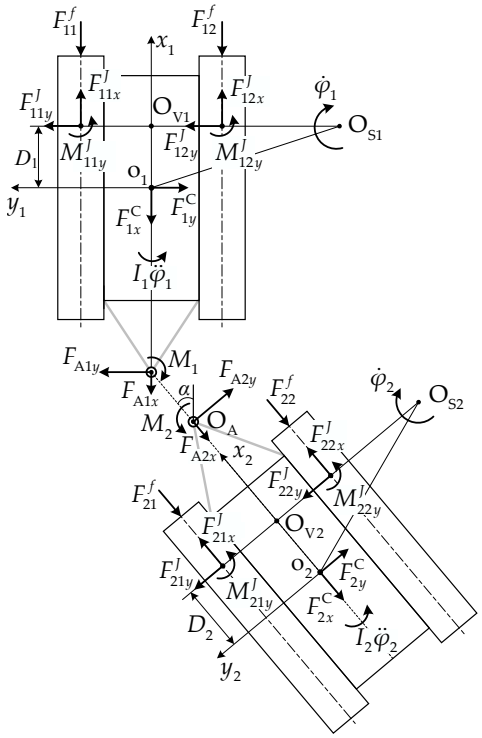


Figure 6. Force diagram of the ATV during a turning motion.

Based on the force equilibrium conditions in the local unit coordinate systems along the x_i and y_i directions, the moment equilibrium conditions around the rotation centers, O_{vi}, of the units can be obtained via the following:

$$\begin{cases} m_i a_{ix} = & F^J_{i1x} + F^J_{i2x} - F^f_{i1} - F^f_{i2} - F_{Aix} \\ m_i a_{1y} = & F^J_{i1y} + F^J_{i2y} \pm F_{Aiy} \\ I_i \ddot{\varphi}_i & = \pm M_i + M^J_{i1x} - M^J_{i2x} - M^J_{i1y} - M^J_{i2y} \\ & \quad -\frac{B}{2}\left(F^f_{i1} - F^f_{i2}\right) - m_i a_{iy} D_i + F_{Aiy}(l_i \pm D_i) \end{cases} \tag{33}$$

Equations (22), (23), (27), (28), and (33) reveal a state of mutual influence and dynamic equilibrium among the mechanical variables, as is demonstrated in Figure 7. The dynamic model includes eight unknowns: A_{11}, A_{12}, A_{21}, A_{22}, D_1, D_2, F_{A1x}, and F_{A1y}. These unknowns can be solved using Equations (31)–(33).

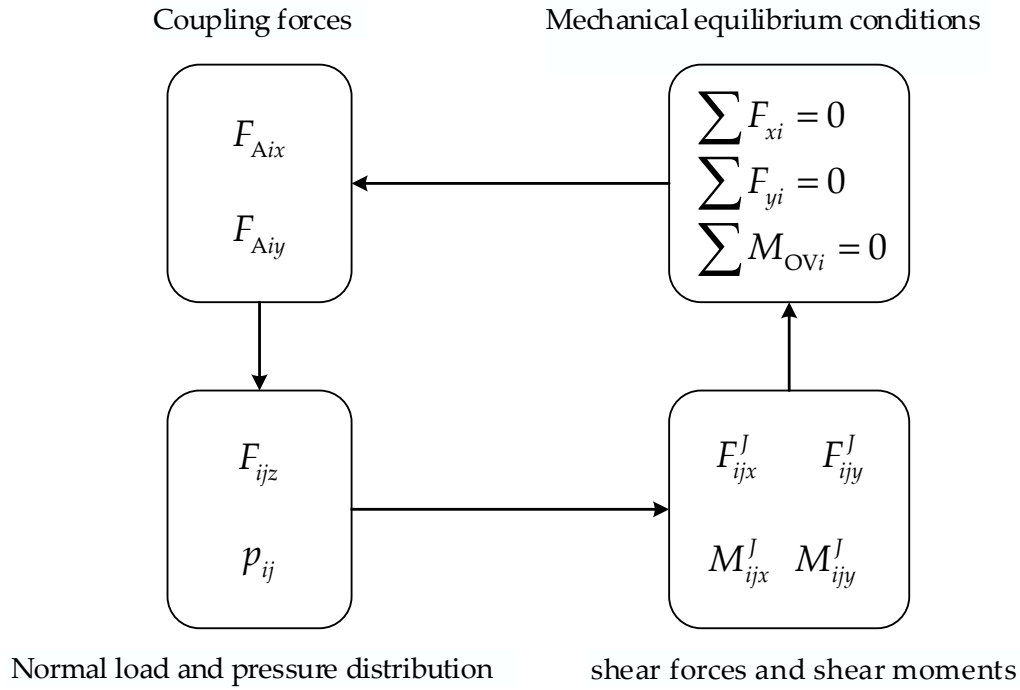


Figure 7. Mechanical interactions in the presence of inter-unit coupling forces.

4. Model Validation and Analysis of the Calculation Results

4.1. Vehicle and Ground Parameters

A calculation example was performed for a certain type of ATV, and the primary parameters of the ATV and the firm ground conditions are listed in Table 1.

Table 1. Parameters of the ATV and the ground.

Parameter	Value	Parameter	Value
m_i	5000 kg	B	2.0 m
h_i	1.5 m	h_A	0.6 m
l_i	2.0 m	r	0.3 m
L_i	3.0 m	μ	0.68
b	0.6 m	K	0.12

4.2. Model Validation

The validity of the turning dynamic model presented in this paper was verified by comparing its results with the theoretical and experimental values of the vehicle thrust to weight ratio, F_{dij}/W_i, and the ratio of the turning radius to the track length, R_i/L_i, provided by Watanabe [7]. The data in Watanabe [7] were obtained on a firm ground by a scale prototype of ATV with $m_1 = m_2 = 55.5$ kg and $L_1 = L_2 = 0.43$ m. According to the range of R_i/L_i values presented by Watanabe [6], results of numerical iteration calculations obtained for steering angles of 25°, 30°, and 35°, as well as speeds in the 0.5–6.0 m/s range, were used for the comparison. The results of the comparison are presented in Figure 8, which demonstrates that the numerical calculation results obtained during this study aligned well with the data in Watanabe [7]. In addition, the RMSE with respect to the numerical data presented by Watanabe [7] was 0.0167, which indicates that the turning dynamic model established during this study can effectively predict ATV turning behavior.

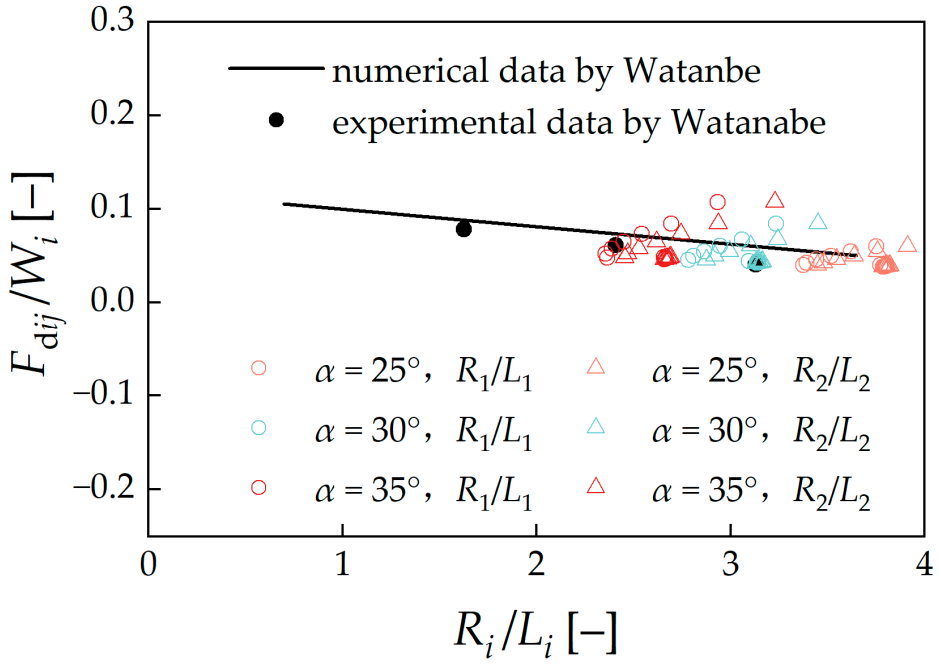


Figure 8. Experimental and numerical relationships between F_{dij}/W_i and R_i/L_i.

4.3. Analysis of the Calculation Results

4.3.1. Unit Rotation Centers

The position changes in the rotation centers of the units can be clearly visualized by changes in the longitudinal offset, D_i. The relationships between D_i of the instantaneous rotation centers of the units, v_1, and α are shown in Figure 9. As both v_1 and α increased, the value of D_2 transitioned from negative to positive. This change indicates that the rotation center of the rear unit shifted from behind to in front of its center of mass, gradually moving closer to the articulation point. D_1 remained consistently positive and exhibited an overall increasing trend at greater speeds; this result suggests that the rotation center of the front unit was always located in front of its center of mass and continued to move further forward as the speed increased. The numerical data for the main kinematic and mechanical parameters at integer speeds are listed in Table A1 in the Appendix A.

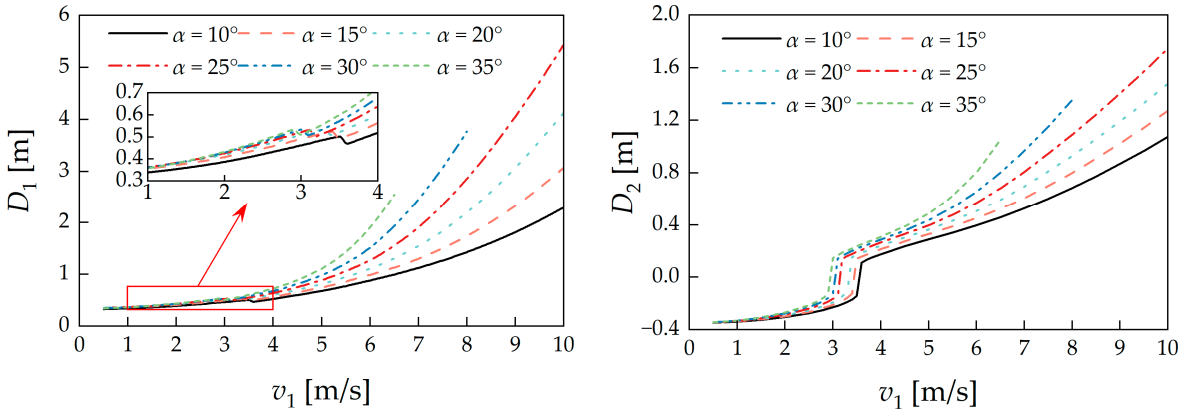


Figure 9. Relationships between D_i, v_1, and α.

4.3.2. Inter-Unit Coupling Forces

Figure 10 depicts the relationships between the inter-unit coupling forces, v_1, and α. When v_1 increased to approximately 6.0 m/s, the longitudinal force, F_{A1x}, acting on the front unit changed direction and transitioned from a resistance that hindered the forward motion of the front unit to a thrust that favored the motion. In contrast, the lateral force, F_{A1y}, consistently provided a driving moment for the turning motion of the front unit. For the rear unit, the longitudinal force, F_{A2x}, increased as α increased when v_1 remained constant, and F_{A2x} always acted as a resistance to the forward motion of the rear unit. As for F_{A1y}, the lateral force acting on the rear unit, F_{A2y}, continuously supplied a driving moment for the turning motion of the rear unit.

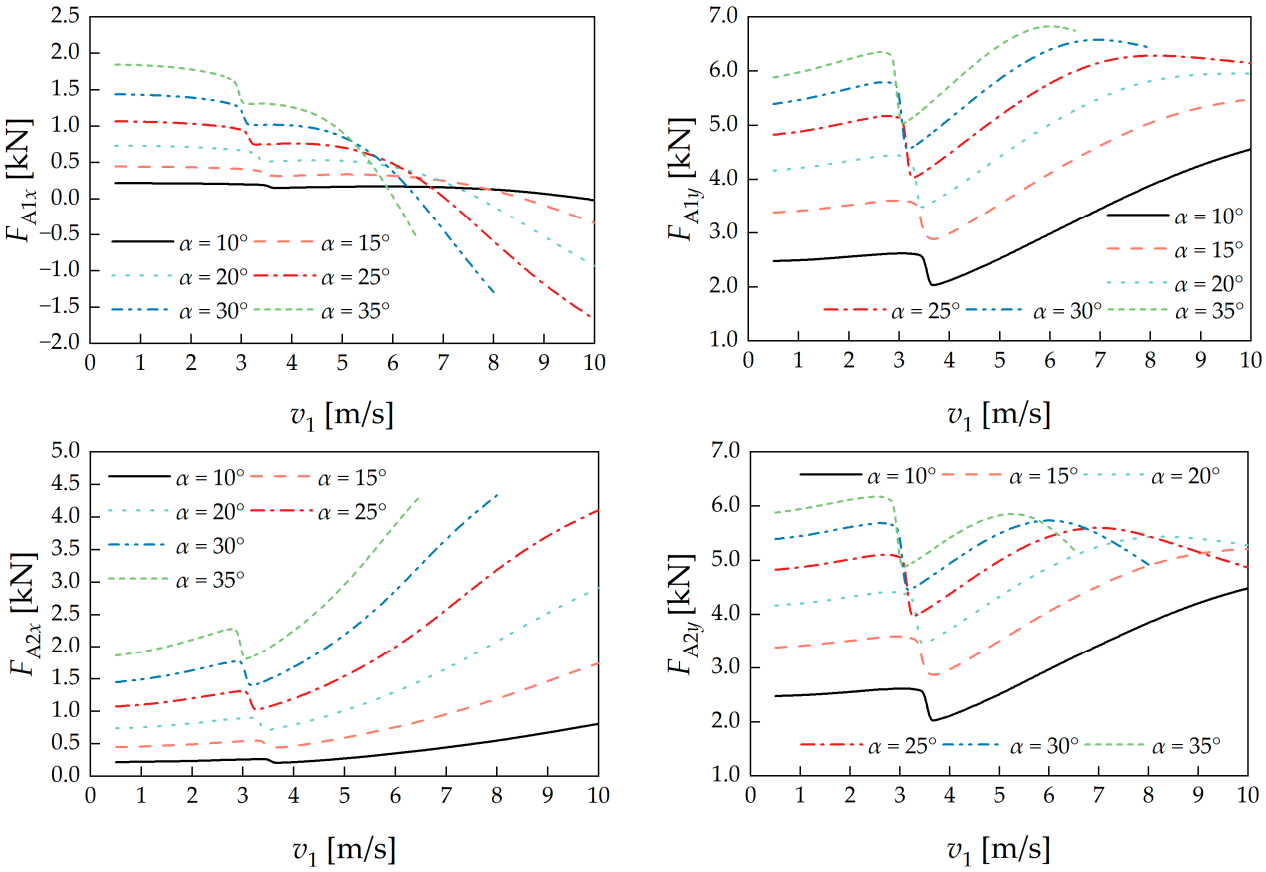


Figure 10. Relationships between the coupling forces, v_1, and α.

5. Effects of the Coupling Forces

By combining the eight unknown turning models from this study with the six unknown turning models from the literature [9–18], which does not consider the load transfer caused by the coupling forces, the effects of the coupling forces on the primary components (such as the front and rear units, the articulation mechanism, and the tracks) were analyzed during an ATV turning process. A steering angle of 25° and speeds in the 0.5–8.0 m/s range were used as examples, and the calculation results of the turning radii of the units, the moments of the articulation mechanism, and the normal loads of the tracks were compared.

5.1. Effects on the Unit Turning Radii

A comparison of the turning radius calculation results obtained by the two modeling methods is presented in Figure 11, where R_i^s is the turning radius obtained without considering the load transfer caused by the coupling forces. Both methods produced R_i and R_i^s values with consistent overall trends. For low-speed turning conditions, in which the rotation center of the rear unit is located behind its center of mass, the changes in R_i and R_i^s with changes in speed were small. In contrast, for high-speed turning conditions, in which the rotation center of the rear unit shifts so that it is in front of the center of mass, significant track sliding and lateral motion caused R_i and R_i^s to increase more rapidly as the speed increased.

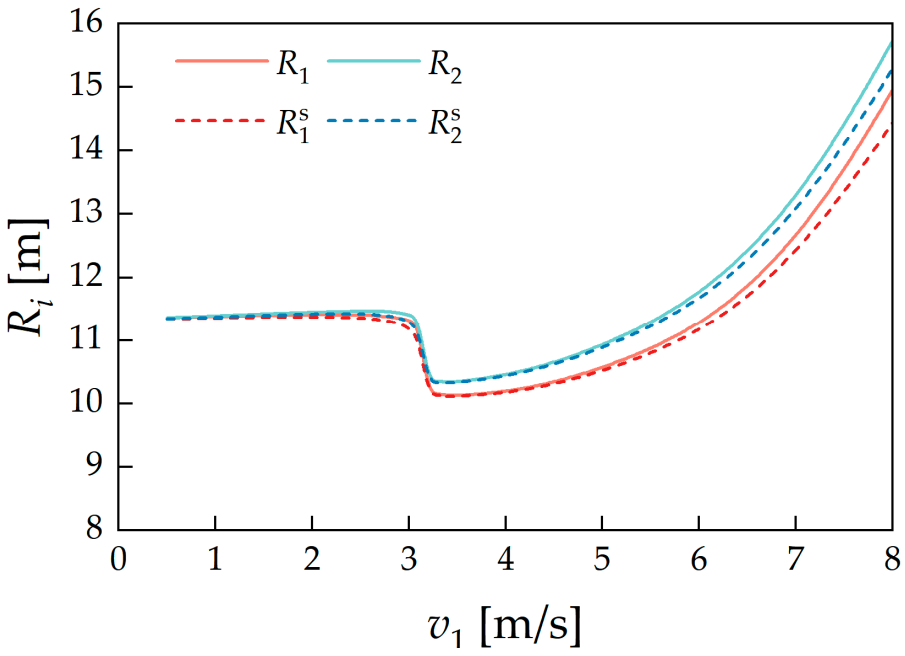


Figure 11. Comparison between the turning radii calculated using both modeling methods.

The effects of the coupling forces on the calculated minimum turning radii of the front and rear units were relatively small; however, the relationship $R_i^s < R_i$ was consistently maintained. At higher speeds, this effect became more pronounced. When the speed reaches 8.0 m/s, the absolute deviations of the calculated turning radii of the front and rear units were 0.53 m and 0.45 m, respectively. This result indicates that considering the load transfer caused by the coupling forces resulted in larger actual turning radii for both units.

5.2. Effects on the Normal Loads of the Tracks

Figure 12 presents a comparison of the track normal load calculation results. When the load transfer caused by the coupling forces is not considered, the track normal load is denoted by F_{ijz}^s. The relationship $F_{i1z}^s > F_{i2z}^s$ was observed, which indicates that the

centrifugal force during the turning process caused the body load to be transferred to the outside track.

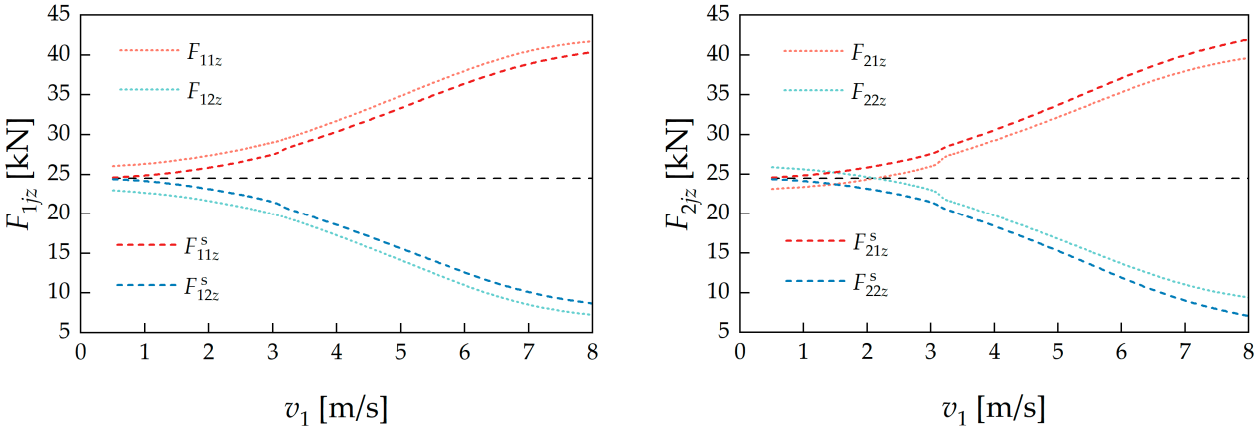


Figure 12. Comparison between the track normal loads calculated using both modeling methods.

The calculated F_{ijz} values demonstrate that the lateral component of the coupling forces caused the unit loads to be transferred to the outer track of the front unit and the inner track of the rear unit. These load transfers resulted in an increased difference between the normal loads of the two tracks of the front unit and a decreased difference between those of the rear unit. In addition, of the four tracks, the outer track of the front unit bore the largest load.

5.3. Effects on the Moment of the Articulation Mechanism

Figure 13 presents a comparison of the calculated moments of the articulation mechanism. When the load transfer caused by the coupling forces is not considered, the moments of the articulation mechanism are denoted by M_{i0}. As the speed increased, the direction of the moment reversed twice. The first reversal occurred when the rotation center of the rear unit passed through the unit center of mass as it shifted from behind to in front of the center of mass.

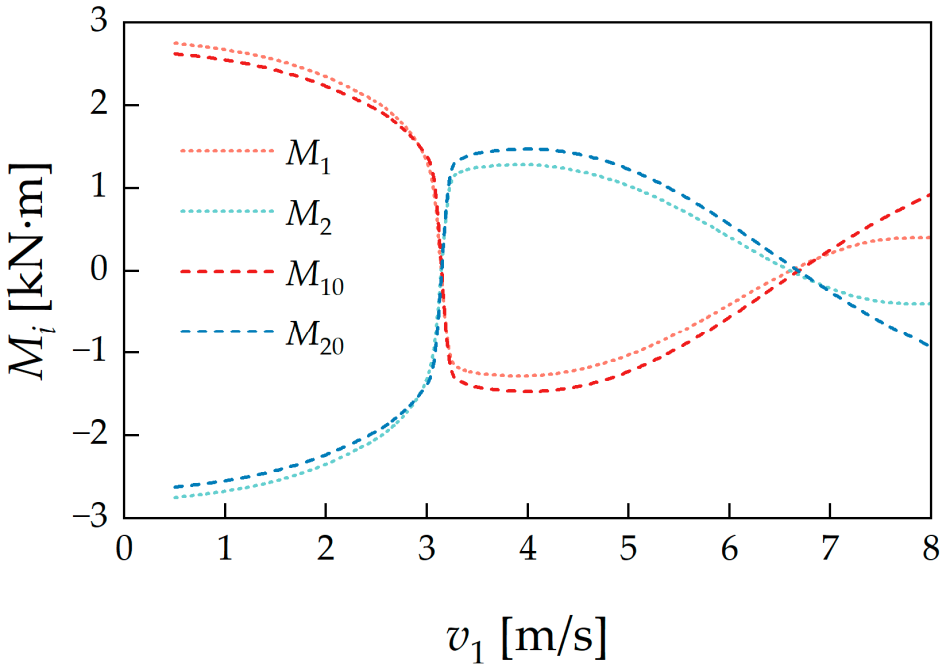


Figure 13. Comparison between the moments of the articulation mechanism.

For low-speed turning conditions, in which the rotation center of the rear unit is located behind the center of mass, the coupling forces increased the moment that the articulation mechanism had to bear. Conversely, for high-speed turning conditions, in which the rotation center is in front of the center of mass, the coupling forces reduced the moment.

6. Analysis of the Turning Performance

6.1. Turning Radius Ratio

During steady-state turning, both the front and rear units share the same turning center; however, the turning radii, R_1 and R_2, of the front and rear units around that center are not equal. The relationships between R_1 and R_2 can be characterized by the turning radius ratio, K_R, which is expressed by Equation (34):

$$K_R = \frac{R_1}{R_2} \tag{34}$$

Figure 14 presents the relationships between K_R, v_1, and α. K_R decreased as both α and v_1 increased, and the relationship $K_R \leq 1$ was maintained throughout the process. This result indicates that the turning radius of the rear unit was larger than that of the front unit during the steady-state turning process.

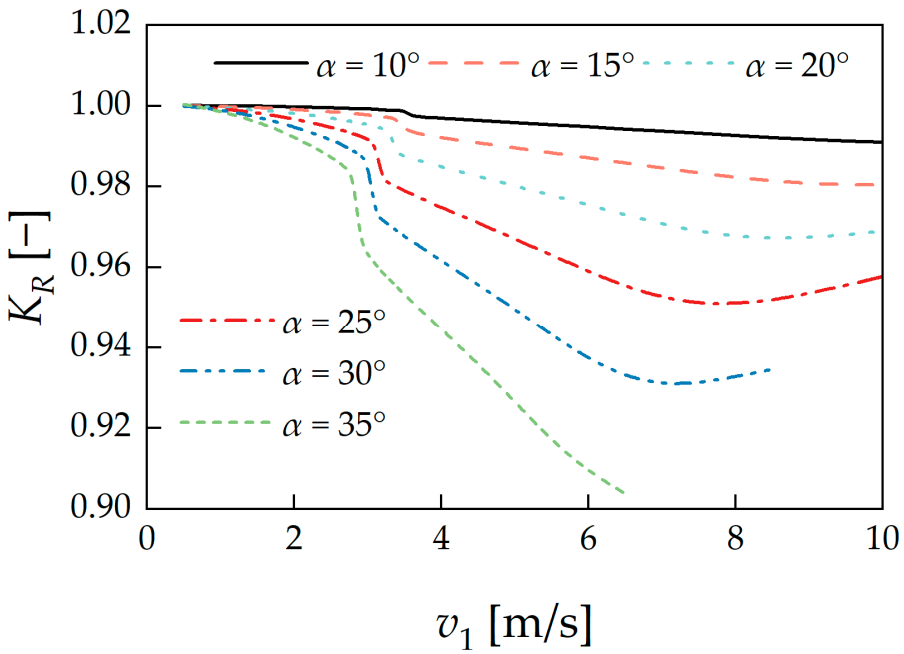


Figure 14. Relationships between K_R, v_1, and α.

6.2. Minimum Swept Radius

Figure 15 presents an analysis of the swept radii during the steady-state turning process. In the local unit coordinate systems, the coordinates of the outer edges of the inner and outer tracks are denoted by $(x_i, \pm(B+b)/2)$. The inner and outer swept radii, which are denoted by R_{in} and R_{out}, respectively, can be expressed by Equation (35):

$$\begin{cases} R_{\text{in}} = \min\sqrt{\left(R_i' - \frac{1}{2}(B+b)\right)^2 + (x_i - D_i)^2} \\ R_{\text{out}} = \max\sqrt{\left[R_i' + \frac{1}{2}(B+b)\right]^2 + (x_i - D_i)^2} \end{cases} \tag{35}$$

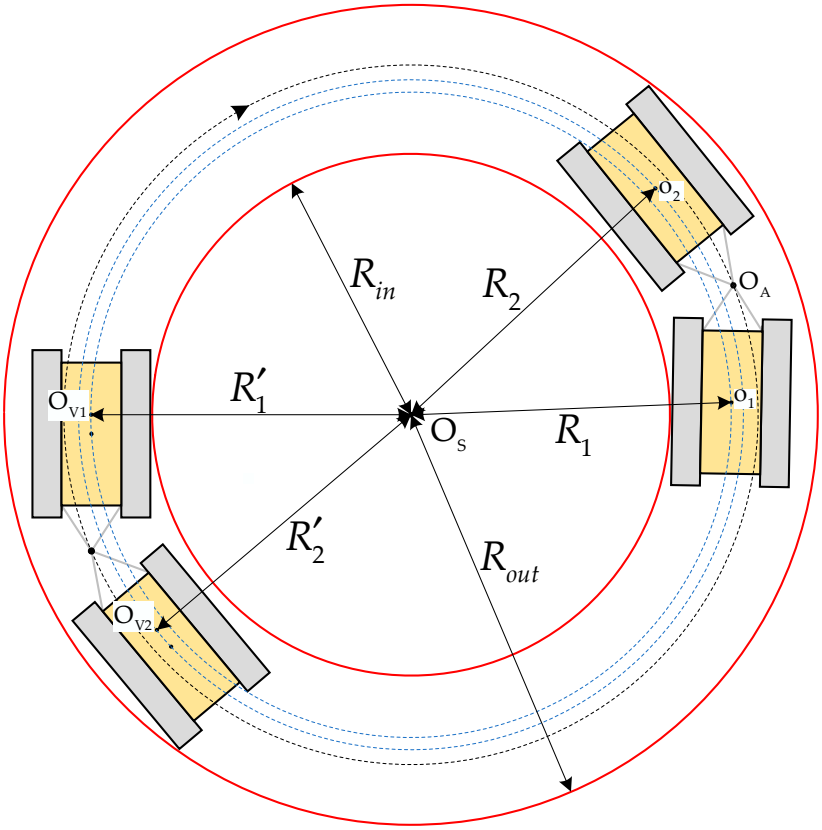


Figure 15. Analysis of the swept radii.

Figure 16 depicts the relationships between R_{in}, v_1, and α. The variations in R_{in} followed the same trend as that of the turning radius depicted in Figure 11. During steady-state turning, R_{in} is dependent upon the radius of the trajectory at point $(\min(D_1, L_1/2), (B+b)/2)$ on the outer edge of the inner track of the front unit.

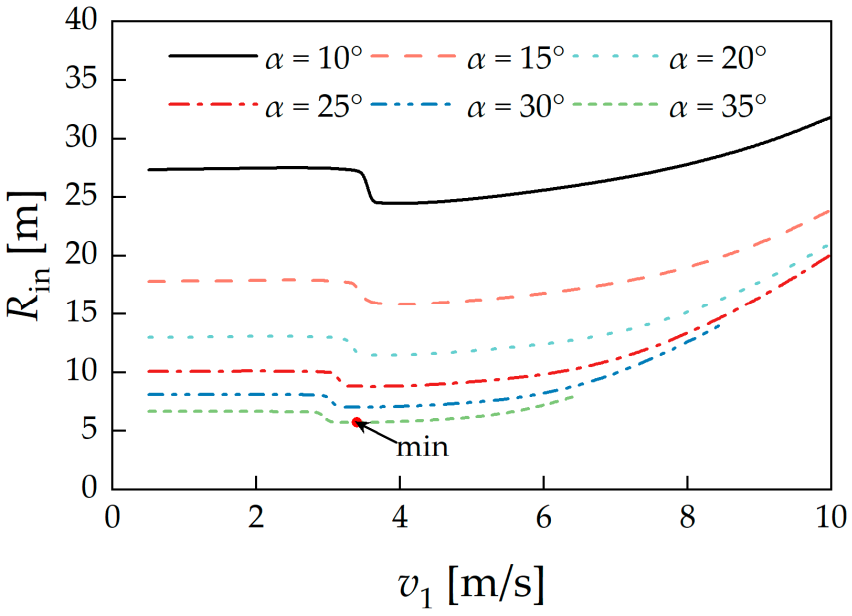


Figure 16. Relationships between R_{in}, v_1, and α.

Figure 17 presents the relationships between R_{out}, v_1, and α. These results are consistent with the calculation results obtained for K_R. The results indicate that R_{out} is dependent upon the maximum trajectory radius of the outer edge of the outer track of the rear unit.

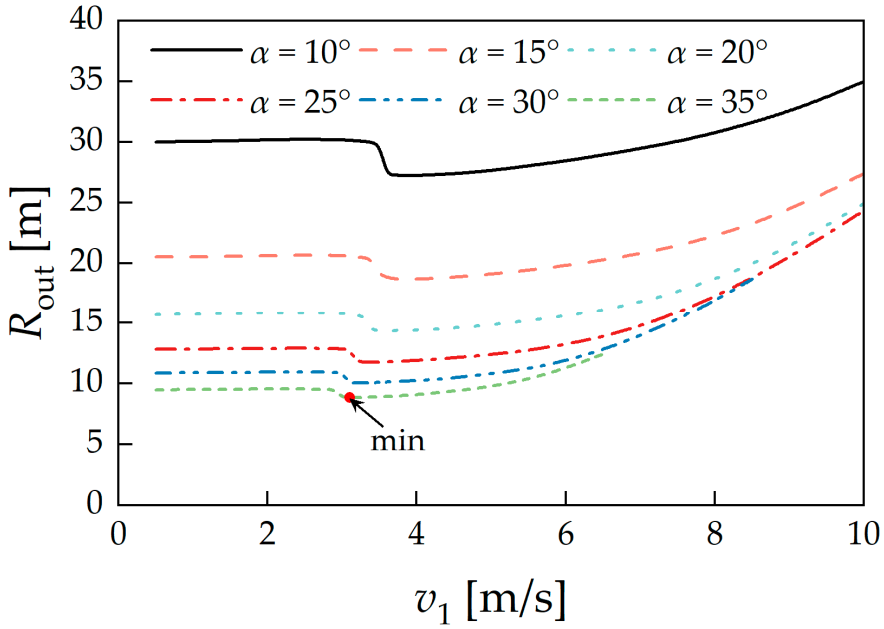


Figure 17. Relationships between R_{out}, v_1, and α.

For low-speed turning conditions, in which the rotation center of the rear unit is behind its center of mass, the coordinates of this critical point are $(L_2/2, -(B+b)/2)$. For high-speed turning conditions, in which the rotation center of the rear unit is in front of its center of mass, the coordinates of this critical point are $(-L_2/2, -(B+b)/2)$. When the ATV has a steering angle of 35° and a speed of 3.1 m/s, the vehicle reaches its minimum outer swept radius of 8.8 m.

6.3. Turning Space

Turning motions performed by the ATV at different steering angles and speeds require different amounts of space. The turning space requirement can be analyzed using the lateral displacement of the rear unit relative to the front unit. This lateral displacement, D_R, can be expressed by Equation (36):

$$D_R = R_{\text{out}} - R_{\text{in}} \tag{36}$$

D_R is influenced by changes in the vehicle dimensions caused by both the steering angle and the side slip angles, β_i. Figure 18 depicts the relationships between β_i, v_1, and α. The side slip angle of the front unit, β_1, increased with increases in both α and v_1. In addition, the calculation results of the side slip angle of the rear unit, β_2, indicate that the head direction deviated least from the motion direction when its rotation center shifted from behind to in front of the center of mass.

Figure 19 presents the relationships between D_R, v_1, and α. It shows that D_R increased as both α and v_1 increased. Additionally, when the ATV operated under the minimum outer swept radius turning condition, D_R was 3.1 m.

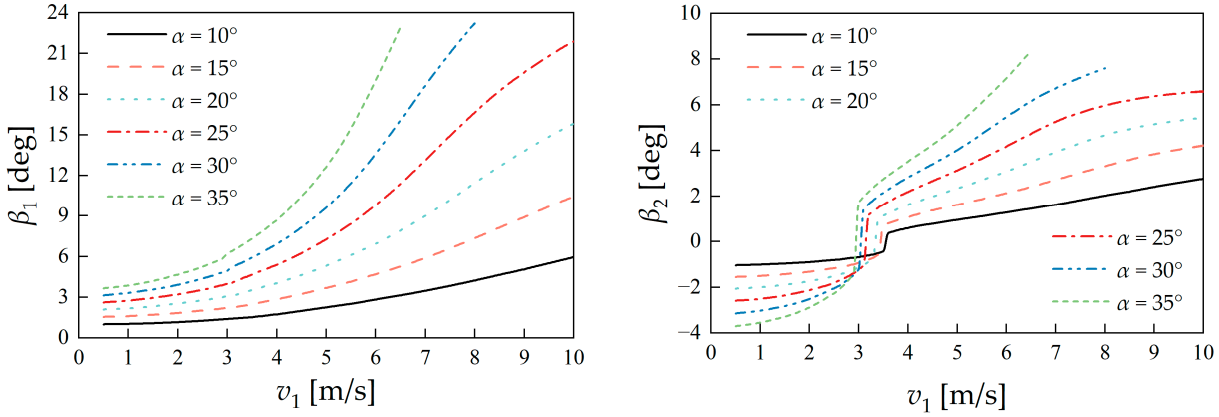


Figure 18. Relationships between β_i, v_1, and α.

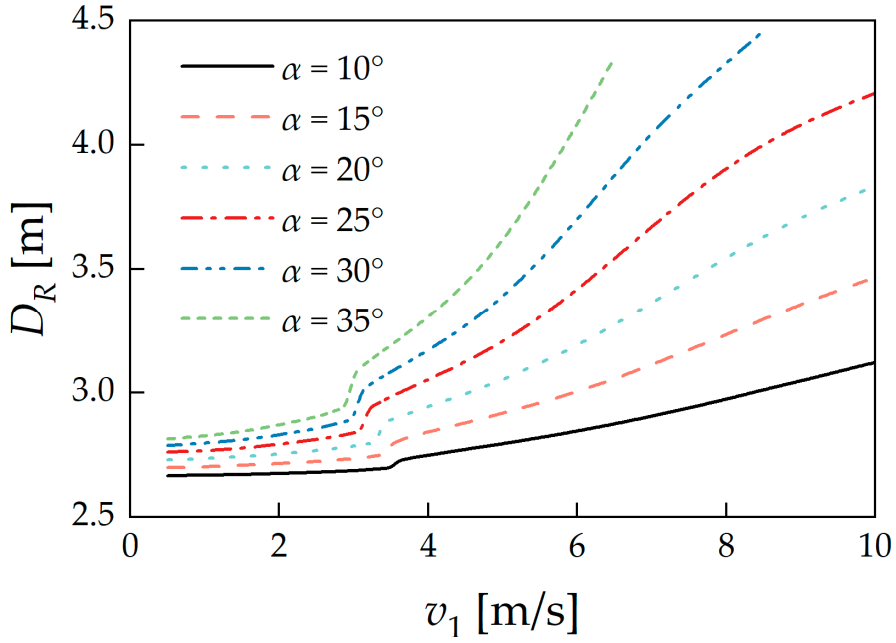


Figure 19. Relationships between D_R, v_1, and α.

7. Conclusions

While considering the load transfer and force transmission caused by inter-unit coupling forces, which were treated as unknown variables, a steady-state turning model for ATVs operating under skidding conditions was developed during this study. The turning model can calculate the kinematic and dynamic parameters of the ATV for various turning conditions, as well as the mechanical interactions between the front and rear sections of the vehicle. The study produced the following three primary conclusions:

(1) The mechanics of the coupling forces and the moments of the articulation mechanism were explored. The lateral components of the coupling forces provided driving moments for the turning motion of each unit, while the longitudinal components provided resistance to the longitudinal motion of both the front and rear sections when the speed was less than 6 m/s. In addition, the moment of the articulation mechanism primarily balanced the unit moments by means of moment compensation.

(2) The effects of the load transfer and force transmission caused by the coupling forces on the ATV turning motions were investigated. It was found that these effects increased the actual turning radius of each vehicle segment and caused the greatest load to be borne by the outer track of the front unit. When the rotation center of the rear unit

was behind its center of mass, the coupling forces increased the moment provided by the articulation mechanism. Conversely, when the rotation center was in front of the center of mass, it decreased the provided moment.

(3) An analysis of the vehicle turning performance revealed that the turning radius of the rear unit was larger than that of the front unit. In addition, the outer swept radius was determined by the path of the outer track of the rear unit, and the lateral displacement increased as both the steering angle and speed increased.

The steady-state turning model established in this study is characterized by its universality and modularity, making it applicable for analyzing the turning performance of other configurations of articulated tracked vehicles. Future research could involve optimizing the design of ATVs to improve the turning performance by adjusting parameters such as the center of mass location, articulation point location, and track dimensions. Moreover, with simple modifications, this model can be adapted for analyzing the turning performance of ATVs on soft terrains like sand or snow, as well as those utilizing distributed drive systems. The analysis of turning performance metrics, including the minimum sweep radius and turning space, provides theoretical support for rapid maneuverability and steering control of vehicles in confined off-road environments, such as jungles and mountainous regions.

Author Contributions: Methodology: N.L. and X.L.; Data curation: N.L. and H.C.; Validation: Y.Z.; Formal analysis: N.L.; Writing—original draft: N.L.; Writing—review and editing: N.L. and H.C.; Supervision: X.L.; Project administration: Y.Z. and X.L. All authors have read and agreed to the published version of the manuscript.

Funding: This research received no external funding.

Data Availability Statement: Data are contained within the article.

Conflicts of Interest: The authors declare no conflicts of interest.

Abbreviations

The following abbreviations are used in this paper:

Parameter Symbol	Parameter Meaning	Parameter Symbol	Parameter Meaning
O_A	articulation point	o_i	centers of mass of the front and rear units
m_i	masses of the front and rear units	L_i	lengths of the track–ground contact sections
l_i	distances between O_A and o_i	B	track center distances
b	track widths	v_i	speeds of o_i
v_{ix}, v_{iy}	longitudinal and lateral speed components of o_i	φ_i	yaw angles of the front and rear units
β_i	side slip angles of the front and rear units	O_{Si}	instantaneous turning centers
R_i	instantaneous turning radii	R_i'	lateral distances between O_{Si} and the longitudinal axes of the units
D_i	longitudinal offsets	α	steering angle
$k_{ij}(x_i, 0)$	point lies on the track longitudinal axis at the track–ground interface	v_{kijx}, v_{kijy}	longitudinal and lateral speed components of k_{ij}
r	radius of the pitch circle of drive wheels	ω_{ij}	angular speeds of the drive wheels
v^J_{kijx}, v^J_{kijy}	longitudinal and lateral components of the sliding speed of k_{ij}	A_{ij}	lateral displacement of the instantaneous center of speed
γ_{ij}	slip angles at k_{ij}	P	direction cosine matrix for the local unit coordinate systems with respect to the global coordinate system
V^J_{kijX}, V^J_{kijY}	sliding speed components of k_{ij} in the global coordinate system	t	time required for point k_{ij} to move from $(L_i/2, 0)$ to $(x_i, 0)$

$J_{X_{ij}}$,$J_{Y_{ij}}$	shear displacements of track *ij* in the X- and Y-directions of the global coordinate system	J_{ij}	total shear displacements of track *ij*
F_{ijz}	normal loads of the tracks	F_{ix}^{C}, F_{iy}^{C}	inertial forces acting on the front and rear units
$F_{\mathrm{A}ix}$, $F_{\mathrm{A}iy}$	longitudinal and lateral components of the coupling forces	h_{A}	distance from $\mathrm{O_A}$ to the ground
h_i	distance from o_i to the ground	p_{ij}	normal pressure of track *ij*
τ	shear stress	μ	friction coefficient
J	shear displacement	K	shear deformation parameter
$\mathrm{d}A_{ij}$	area of a differential element at the track–ground interface of track *ij*	$\mathrm{d}F_{ijx}^{J}$, $\mathrm{d}F_{ijy}^{J}$	longitudinal force and lateral force components on $\mathrm{d}A_{ij}$
F_{ijx}^{J}, F_{ijy}^{J}	total longitudinal and lateral shear forces	M_{ijx}^{J}, M_{ijy}^{J}	longitudinal and lateral shear moment
$\mathrm{O}_{\mathrm{v}i}$	rotation center of the front and rear units	F_{ij}^{f}	external track motion resistance
f_r	external motion resistance coefficient	T_{ij}	output torques from the driving wheels
I_{d}	moment of inertia of the driving wheel	I_{w}	moment of inertia of the load wheel
$\dot{\omega}_{\mathrm{w}ijk}$	rolling angular speed of the k_{th} load wheel	v_{ijk}	rolling linear speed of the k_{th} load wheel
f_0, f_s	empirical coefficients	$F_{\mathrm{d}ij}$	driving force of track *ij*
M_i	moments of the articulation mechanism	M_{i0}	moments of the articulation mechanism without considering the load transfer caused by the coupling forces
F_{ijz}^{s}	track normal loads without considering the load transfer caused by the coupling forces	K_R	turning radius ratio
R_{in}, R_{out}	inner and outer swept radii	D_R	lateral displacement of the rear unit relative to the front unit

Appendix A

Table A1. Numerical data for the main kinematic and mechanical parameters at integer speeds.

Input								**Output**							
α **(deg)**	v_1 **(m/s)**	v_2 **(m/s)**	R_1 **(m)**	R_2 **(m)**	φ_i **(deg/s)**	β_1 **(deg)**	β_2 **(deg)**	F_{11z} **(kN)**	F_{12z} **(kN)**	F_{21z} **(kN)**	F_{22z} **(kN)**	M_1 **(kN)**	M_2 **(kN)**	$F_{\mathrm{A}1x}$ **(kN)**	$F_{\mathrm{A}1y}$ **(kN)**
10	1.00	1.00	28.67	28.67	1.98	1.01	−1.02	25.38	23.62	23.88	25.12	1.46	−1.46	0.21	2.49
	2.00	2.00	28.78	28.79	3.95	1.15	−0.91	25.79	23.21	24.26	24.74	1.27	−1.27	0.21	2.56
	3.00	3.00	28.78	28.80	5.92	1.38	−0.69	26.46	22.54	24.89	24.11	0.86	−0.86	0.20	2.62
	4.00	4.01	25.76	25.84	8.82	1.73	0.59	27.46	21.54	26.20	22.80	−0.97	0.97	0.15	2.12
	5.00	5.02	26.15	26.26	10.86	2.23	0.95	28.84	20.16	27.35	21.65	−1.26	1.26	0.17	2.52
	6.00	6.03	26.93	27.07	12.65	2.81	1.26	30.40	18.60	28.65	20.35	−1.43	1.43	0.17	2.99
	7.00	7.04	27.90	28.07	14.25	3.46	1.62	32.11	16.89	30.10	18.90	−1.43	1.43	0.16	3.45
	8.00	8.06	29.15	29.37	15.58	4.21	2.01	33.88	15.12	31.63	17.37	−1.31	1.31	0.13	3.89
	9.00	9.08	30.90	31.16	16.54	5.05	2.40	35.57	13.43	33.14	15.86	−1.16	1.16	0.07	4.27
	10.00	10.09	33.28	33.59	17.06	5.94	2.75	37.07	11.93	34.51	14.49	−1.03	1.03	−0.02	4.56
15	1.00	1.00	19.14	19.14	2.97	1.60	−1.51	25.72	23.28	23.67	25.33	1.94	−1.94	0.44	3.42
	2.00	2.00	19.21	19.23	5.91	1.83	−1.33	26.34	22.66	24.23	24.77	1.68	−1.68	0.43	3.52
	3.00	3.01	19.18	19.22	8.88	2.20	−0.94	27.34	21.66	25.19	23.81	1.10	−1.10	0.41	3.61
	4.00	4.03	17.12	17.25	13.27	2.83	1.07	28.90	20.10	27.14	21.86	−1.33	1.33	0.32	2.98
	5.00	5.05	17.48	17.66	16.24	3.67	1.61	30.91	18.09	28.86	20.14	−1.54	1.54	0.34	3.54
	6.00	6.08	18.14	18.37	18.78	4.67	2.12	33.15	15.85	30.82	18.18	−1.50	1.50	0.32	4.12
	7.00	7.11	19.05	19.35	20.87	5.88	2.70	35.48	13.52	32.93	16.07	−1.22	1.22	0.25	4.63
	8.00	8.14	20.45	20.82	22.21	7.33	3.31	37.66	11.34	34.96	14.04	−0.87	0.87	0.12	5.05
	9.00	9.18	22.56	23.00	22.66	8.91	3.83	39.40	9.60	36.66	12.34	−0.55	0.55	−0.09	5.33
	10.00	10.20	25.44	25.95	22.32	10.44	4.22	40.64	8.36	37.93	11.07	−0.30	0.30	−0.34	5.48

Table A1. *Cont.*

Input								Output							
α (deg)	v_1 (m/s)	v_2 (m/s)	R_1 (m)	R_2 (m)	φ_i (deg/s)	β_1 (deg)	β_2 (deg)	F_{11z} (kN)	F_{12z} (kN)	F_{21z} (kN)	F_{22z} (kN)	M_1 (kN)	M_2 (kN)	F_{A1x} (kN)	F_{A1y} (kN)
20	1.00	1.00	14.31	14.31	3.97	2.17	−2.01	26.02	22.98	23.50	25.50	2.29	−2.29	0.73	4.20
	2.00	2.00	14.36	14.39	7.91	2.51	−1.74	26.85	22.15	24.25	24.75	2.00	−2.00	0.71	4.34
	3.00	3.01	14.29	14.36	11.92	3.06	−1.14	28.19	20.81	25.55	23.45	1.28	−1.28	0.66	4.44
	4.00	4.06	12.79	12.98	17.76	4.04	1.60	30.31	18.69	28.15	20.85	−1.50	1.50	0.53	3.76
	5.00	5.10	13.15	13.42	21.59	5.32	2.33	32.92	16.08	30.47	18.53	−1.52	1.52	0.53	4.42
	6.00	6.15	13.79	14.14	24.70	6.93	3.08	35.73	13.27	33.06	15.94	−1.18	1.18	0.45	5.03
	7.00	7.21	14.84	15.29	26.78	9.00	3.92	38.38	10.62	35.65	13.35	−0.62	0.62	0.24	5.51
	8.00	8.27	16.64	17.19	27.31	11.42	4.66	40.39	8.61	37.73	11.27	−0.07	0.07	−0.10	5.82
	9.00	9.30	19.30	19.96	26.47	13.79	5.15	41.56	7.44	39.08	9.92	0.33	−0.33	−0.53	5.94
	10.00	10.32	22.73	23.46	24.98	15.82	5.43	42.16	6.84	39.87	9.13	0.61	−0.61	−0.93	5.95
25	1.00	1.00	11.38	11.39	4.99	2.74	−2.51	26.29	22.71	23.37	25.63	2.56	−2.56	1.06	4.88
	2.00	2.01	11.41	11.45	9.95	3.21	−2.13	27.33	21.67	24.31	24.69	2.25	−2.25	1.04	5.06
	3.00	3.02	11.31	11.41	15.06	3.97	−1.25	29.02	19.98	25.99	23.01	1.39	−1.39	0.95	5.14
	4.00	4.10	10.18	10.44	22.32	5.39	2.18	31.71	17.29	29.23	19.77	−1.49	1.49	0.76	4.47
	5.00	5.17	10.56	10.92	26.89	7.26	3.13	34.86	14.14	32.17	16.83	−1.25	1.25	0.71	5.18
	6.00	6.26	11.26	11.74	30.26	9.78	4.18	38.05	10.95	35.33	13.67	−0.57	0.57	0.50	5.78
	7.00	7.35	12.63	13.26	31.48	13.12	5.25	40.52	8.48	38.03	10.97	0.26	−0.26	0.04	6.17
	8.00	8.41	14.96	15.73	30.36	16.64	5.97	41.76	7.24	39.64	9.36	0.93	−0.93	−0.59	6.29
	9.00	9.44	18.12	19.00	28.21	19.60	6.36	42.17	6.83	40.43	8.57	1.37	−1.37	−1.19	6.24
	10.00	10.44	21.89	22.86	25.94	21.89	6.59	42.24	6.76	40.80	8.20	1.66	−1.66	−1.67	6.15
30	1.00	1.00	9.41	9.42	6.03	3.30	−3.02	26.54	22.46	23.26	25.74	2.75	−2.75	1.43	5.46
	2.00	2.01	9.43	9.48	12.04	3.91	−2.51	27.79	21.21	24.41	24.59	2.46	−2.46	1.39	5.68
	3.00	3.04	9.28	9.41	18.35	4.95	−1.21	29.84	19.16	26.51	22.49	1.42	−1.42	1.25	5.71
	4.00	4.16	8.42	8.76	26.96	6.93	2.82	33.11	15.89	30.42	18.58	−1.33	1.33	1.02	5.12
	5.00	5.27	8.84	9.31	32.12	9.62	4.03	36.72	12.28	33.99	15.01	−0.75	0.75	0.87	5.86
	6.00	6.40	9.71	10.36	35.10	13.57	5.46	39.94	9.06	37.55	11.45	0.31	−0.31	0.40	6.41
	7.00	7.52	11.55	12.41	34.42	18.63	6.73	41.56	7.44	39.83	9.17	1.38	−1.38	−0.43	6.59
	8.00	8.58	14.34	15.37	31.68	23.21	7.61	41.81	7.19	40.81	8.19	2.05	−2.05	−1.29	6.43
35	1.00	1.00	7.99	8.00	7.11	3.85	−3.55	26.76	22.24	23.19	25.81	2.87	−2.87	1.84	5.97
	2.00	2.02	8.00	8.06	14.19	4.65	−2.88	28.24	20.76	24.55	24.45	2.63	−2.63	1.78	6.23
	3.00	3.11	7.10	7.37	24.00	6.19	1.69	30.73	18.27	27.98	21.02	−1.17	1.17	1.31	5.00
	4.00	4.23	7.17	7.59	31.70	8.71	3.51	34.49	14.51	31.72	17.28	−1.02	1.02	1.27	5.72
	5.00	5.40	7.63	8.24	37.20	12.63	5.10	38.43	10.57	35.95	13.05	−0.03	0.03	0.94	6.49
	6.00	6.60	8.81	9.69	38.69	18.97	7.15	41.06	7.94	39.53	9.47	1.48	−1.48	0.05	6.87

References

1. Nuttall, C.J. Some Notes on the Steering of Tracked Vehicles by Articulation. *J. Terramech.* **1964**, *1*, 38–74. [CrossRef]
2. Alhimdani, F.F. Steering Analysis of Articulated Tracked Vehicles. *J. Terramech.* **1982**, *19*, 195–209. [CrossRef]
3. Zhang, Y.; Liu, X.; Chen, H.; Qiu, M.; Zhao, Y.; Zhang, X. Slope-Steering Motion Planning for Unmanned Tracked Vehicles Based on SSTP-RRT. *IEEE Access* **2024**, *12*, 1–20. [CrossRef]
4. Tang, S.; Yuan, S.; Hu, J.; Li, X.; Zhou, J.; Guo, J. Modeling of Steady-State Performance of Skid-Steering for High-Speed Tracked Vehicles. *J. Terramech.* **2017**, *73*, 25–35. [CrossRef]
5. Liu, W. Research on Fatigue and Initial Track Tension Optimization of the Track for an All-Terrain Articulated Tracked Vehicle. Ph.D. Thesis, School of Mechanical and Aerospace Engineering, Jilin University, Changchun, China, 2021.
6. Yugang, L.; Guangjun, L. Modeling of Tracked Mobile Manipulators with Consideration of Track-Terrain and Vehicle-Manipulator Interactions. *Robot. Auton. Syst.* **2009**, *57*, 1065–1074.
7. Watanabe, K.; Kitano, M. Study on Steerability of Articulated Tracked Vehicles—Part 1. Theoretical and Experimental Analysis. *J. Terramech.* **1986**, *23*, 69–83. [CrossRef]
8. Yamakawa, J.; Watanabe, K.; Inagaki, T.; Kitano, M.; Jozaki, H. Turning Characteristics of Articulated Tracked-Vehicles. *Trans. JSME Part C* **2000**, *66*, 579–585. [CrossRef]
9. Yamakawa, J.; Watanabe, K.; Yasuda, Y. Turning Characteristics of Articulated Tracked Vehicles (Vehicle Characteristics and Steering Performance). *Trans. JSME Part C* **2001**, *67*, 1544–1551. [CrossRef]
10. Tota, A.; Velardocchia, M.; Rota, E.; Novara, A. *Steering Behavior of an Articulated Amphibious All-Terrain Tracked Vehicle*; 2020-01-0996; SAE Technical Paper; SAE International: Warrendale, PA, USA, 2020.
11. Tota, A.; Galvagno, E.; Velardocchia, M. Analytical Study on the Cornering Behavior of an Articulated Tracked Vehicle. *Machines* **2021**, *9*, 38. [CrossRef]

12. Dong, C.; Cheng, K.; Hu, W.; Yao, Y. Dynamic Modelling of the Steering Performance of an Articulated Tracked Vehicle Using Shear Stress Analysis of the Soil. *Proc. Inst. Mech. Eng. Part D J. Automob. Eng.* **2017**, *231*, 653–683. [CrossRef]
13. Dong, C.; Cheng, K.; Hu, K.; Hu, W. Dynamic Modeling Study on the Slope Steering Performance of Articulated Tracked Vehicles. *Adv. Mech. Eng.* **2017**, *9*, 457–482. [CrossRef]
14. Yao, Y.; Cheng, K.; Zhang, B.; Lin, J.; Jiang, D.; Gao, Z. A Steering Model for Articulated Tracked Vehicle Considering Soil Deformation on Track-Soil Interaction. *Adv. Mech. Eng.* **2018**, *10*, 1–11. [CrossRef]
15. Wu, J.; Wang, G.; Zhao, H.; Sun, K. Study on Electromechanical Performance of Steering of the Electric Articulated Tracked Vehicles. *J. Mech. Sci. Tech.* **2019**, *33*, 3171–3185. [CrossRef]
16. Hu, K.; Cheng, K. Dynamic Modelling and Stability Analysis of the Articulated Tracked Vehicle Considering Transient Track-Terrain Interaction. *J. Mech. Sci. Tech.* **2021**, *35*, 1343–1356. [CrossRef]
17. Hu, K. Study on the Dynamics Analysis and Path Tracking Control for Articulated Tracked Vehicles. Ph.D. Thesis, School of Mechanical and Aerospace Engineering, Jilin University, Changchun, China, 2024.
18. Lin, H. Research on Key Control Technologies of Articulated Steering Tracked Vehicle. Ph.D. Thesis, Institute of Automation, Chinese Academy of Sciences, Beijing, China, 2016.
19. Merritt, H.E. Some considerations influencing the design of highspeed track-vehicles. *Proc. Inst. Automob. Eng.* **1939**, *33*, 398–430.
20. Purdy, D.J.; Wormell, P.J.H. Handling of high-speed tracked vehicles. *J. Battlef. Technol.* **2003**, *6*, 17–22.
21. Crosheck, J. *Skid Steering of Crawlers*; SAE Technical Paper 750552; SAE International: Warrendale, PA, USA, 1975.
22. Kitano, M.; Kuma, M. An analysis of horizontal plane motion of tracked vehicles. *J. Terramech.* **1977**, *14*, 211–225. [CrossRef]
23. Galvagno, E.; Rondinelli, E.; Velardocchia, M. Electro-mechanical transmission modelling for series-hybrid tracked tanks. *Int. J. Heavy Vehicle Syst.* **2012**, *19*, 256–280. [CrossRef]
24. Maclaurin, B. A skid steering model with track pad flexibility. *J. Terramechanics* **2007**, *44*, 95–110, Erratum in *J. Terramechanics* **2007**, *44*, 217–218. [CrossRef]
25. Wong, J.Y.; Chiang, C.F. A General Theory for Skid Steering of Tracked Vehicles on Firm Ground. *Proc. Inst. Mech. Eng. Part D J. Automob. Eng.* **2001**, *215*, 343–355. [CrossRef]
26. Wong, J.Y. *Theory of Ground Vehicles*, 4th ed.; Jia, Z.Z.; Li, S.B.; Hu, X.S., Translators; China Machine Press: Beijing, China, 2018.
27. Wang, H.Y.; Wang, Q.L.; Rui, Q.; Gai, H.T.; Zhou, G.M.; Wan, L.; Zhang, F. Analyzing and Testing Verification the Performance about High-Speed Tracked Vehicles in Steering Process. *J. Mech. Eng.* **2014**, *50*, 162–172. [CrossRef]
28. Rui, Q.; Wang, H.Y.; Wang, Q.L.; Guo, J.; Zou, T.G.; Wan, L. Analysis and Experiment of Tracked Vehicle Steering Torque Based on Shear Stress Model. *Acta Armamentarii* **2015**, *36*, 968–977.
29. Wang, H.Y.; Chen, B.; Rui, Q.; Guo, J.; Shi, L.C. Analysis and Experiment of Steady-State Steering of Tracked Vehicle under Concentrated Load. *Acta Armamentarii* **2016**, *37*, 2196–2204.
30. Islam, M.M.; Ding, X.; He, Y. A closed-loop dynamic simulation-based design method for articulated heavy vehicles with active trailer steering systems. *Veh. Syst. Dyn.* **2011**, *50*, 675–697. [CrossRef]
31. Vella, A.D.; Lisitano, D.; Tota, A.; Wang, B. Analysis of heavy commercial vehicle cornering behaviour through a multibody model. *Int. J. Mech. Control* **2020**, *21*, 39–50.
32. Wu, D.H.; Hai, J. Analysis of dynamic lateral response for a multi-axle-steering tractor and trailer. *Int. J. Heavy Veh. Syst.* **2003**, *10*, 281–294. [CrossRef]
33. Gao, Y.; Gordon, T. Optimal control of vehicle dynamics for the prevention of road departure on curved roads. *IEEE Trans. Vehicular Technol.* **2019**, *68*, 9370–9384. [CrossRef]
34. Wang, B.; Liao, Z.; Guo, S. Adaptive curve passing control in autonomous vehicles with integrated dynamics and camera-based radius estimation. *Vehicles* **2024**, *6*, 1648–1660. [CrossRef]
35. Bakibillah, A.S.M.; Kamal, M.A.S.; Tan, C.P.; Hayakawa, T.; Imura, J. Optimal eco-driving scheme for reducing energy consumption and carbon emissions on curved roads. *Heliyon* **2023**, *10*, e23586. [CrossRef]
36. Zheng, B.; Huang, X.; Tang, J.; Chen, J.; Zhao, R.; Hong, Z.; Tang, T.; Han, M. Evaluation on braking stability of autonomous vehicles running along curved sections based on asphalt pavement adhesion properties. *J. Adv. Transp.* **2022**, *2022*, 7348554. [CrossRef]
37. Li, J.F.; Fan, Z.Y.; Fan, F.M. Analysis of Moving Resistance Coefficient and Moving System Efficiency of Tracked Vehicle. *Vehicle Power Technol.* **2015**, *1–4*, 9.

Disclaimer/Publisher's Note: The statements, opinions and data contained in all publications are solely those of the individual author(s) and contributor(s) and not of MDPI and/or the editor(s). MDPI and/or the editor(s) disclaim responsibility for any injury to people or property resulting from any ideas, methods, instructions or products referred to in the content.